Isolating α-Pinene Ozonolysis Pathways Reveals New Insights into Peroxy Radical Chemistry and Secondary Organic Aerosol Formation

Zixu Zhao,[1] Wen Zhang,[1] Taylor Alexander,[1] Xuan Zhang,[2] David B. C. Martin,[1,3] Haofei Zhang[1*]

[1] Department of Chemistry, University of California, Riverside, CA 92521, USA

[2] Department of Life and Environmental Sciences, University of California, Merced, CA 95343, USA

[3] Department of Chemistry, University of Iowa, Iowa City, IA 52242, USA

*Corresponding Author: Haofei Zhang (haofei.zhang@ucr.edu)

Abstract

α-Pinene ozonolysis is a key process that impacts the formation of new particles and secondary organic aerosol (SOA) in the atmosphere. The mechanistic understanding of this chemistry has been inconclusive despite extensive research, hindering accurate simulations of atmospheric processes. In this work, we examine the ozonolysis of two synthesized unsaturated carbonyl isomers ($C_{11}H_{18}O$) which separately produce the two Criegee intermediates (CIs) that would form simultaneously in α-pinene ozonolysis. Direct gas-phase measurements of peroxy radicals (RO_2) from flowtube ozonolysis experiments by an iodide-adduct chemical ionization mass spectrometer suggest that the initial $C_{10}H_{15}O_4$• RO_2 from the CI with a terminal methyl ketone undergo autoxidation twentyfold faster than the CI with a terminal aldehyde and always outcompete the bimolecular reactions under typical laboratory and atmospheric conditions. These results provide experimental constraints on the detailed RO_2 autoxidation mechanisms for understanding new particle formation in the atmosphere. Further, isomer-resolved characterization of the SOA formed from a continuous-flow stirred tank reactor using ion mobility spectrometry mass spectrometry suggests that the two structurally different CIs predominantly and unexpectedly form constituents with identical structures. These results open up possibilities of diverse isomerization pathways that the two CIs may undergo that form mutual products to a large extent toward their way forming the SOA. This work highlights new insights into α-pinene ozonolysis pathways and call for future studies to uncover the detailed mechanisms.

28 TOC:

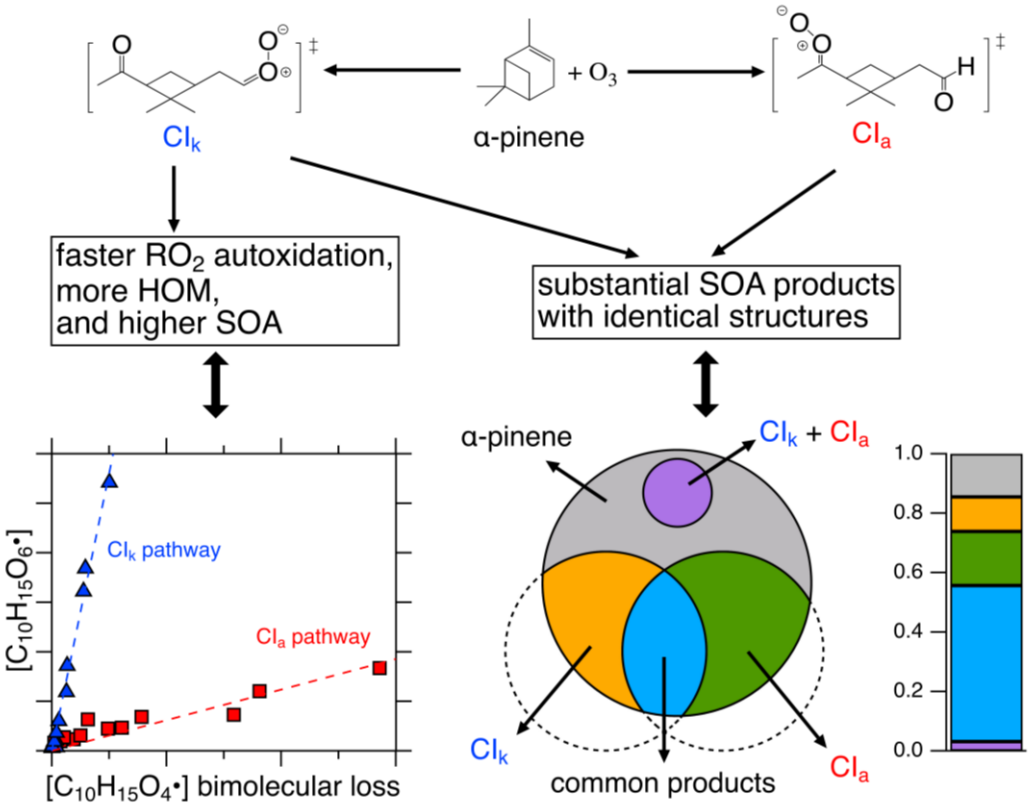
+ O3
α-pinene
CIk
CIa
faster RO2 autoxidation, more HOM, and higher SOA
substantial SOA products with identical structures
[C10H15O6•]
CIk pathway
CIa pathway
[C10H15O4•] bimolecular loss
α-pinene
CIk + CIa
CIk
CIa
common products
1.0
0.8
0.6
0.4
0.2
0.0

29

Introduction

Ozonolysis of monoterpenes is an important reaction in the atmosphere that has significant implications for new particle formation, growth, and secondary organic aerosol (SOA), especially in forested regions such as the boreal forest and southeastern United States.[1-6] Monoterpene ozonolysis starts from the cycloaddition of O_3 to a C=C double bond to form a primary ozonide. In the case of α-pinene ($C_{10}H_{16}$), which is the most abundant monoterpene in the atmosphere,[7] the primary ozonide decomposes into two isomeric energized Criegee intermediates (CIs), as shown in **Figure 1A**.[1] Prior studies have suggested that a large fraction (~ 60 – 90%) of each CI undergoes unimolecular H-shift, followed by O_2 addition, to form the vinyl hydroperoxides (VHP) which subsequently release OH radicals and produce peroxy radicals (RO_2, $C_{10}H_{15}O_4$•) in the presence of O_2.[8-12] $C_{10}H_{15}O_4$• thereafter initiate a series of competing unimolecular (i.e., H-shift followed by O_2 addition, also known as RO_2 autoxidation)[4, 13-14] and multi-generational bimolecular reactions[15] (**Figure 1B**), the products of which may exhibit a wide range of functionalities and volatilities, and thus be present in both the gas and/or particle phases.

The RO_2 autoxidation has been proposed to account for atmospheric new particle formation and growth,[4, 16-18] as well as to contribute to total organic aerosol mass.[6, 14] Prior laboratory studies have suggested that a small fraction (10 – 15%) of $C_{10}H_{15}O_4$• has to autoxidize rapidly (rate constants on the order of 1 s^{-1} or higher) to explain the observed highly oxygenated multifunctional (HOM) products.[4, 19] In contrast, computational calculations suggest that the currently-known $C_{10}H_{15}O_4$• undergo H-shift at much slower rate constants (10^{-9} – 0.29 s^{-1}) due to the strained cyclobutyl ring.[20] To reconcile such a large discrepancy, Kurtén et al. indicated that unrecognized mechanism(s) must exist to lead to ring-opened $C_{10}H_{15}O_4$• that more readily undergoes autoxidation.[20] Recently, Iyer et al. proposed a ring-opening mechanism from one of the CIs (CI_k

in **Figure 1A**) which leads to a ring-opened $C_{10}H_{15}O_4$• that autoxidizes much more rapidly.[21] Experimental evidence for such rapid $C_{10}H_{15}O_4$• autoxidation would be crucial for improving RO_2 autoxidation mechanisms applied in current atmospheric and climate models.[22-23] In addition to the elusive RO_2 autoxidation pathways, the bimolecular RO_2 pathways (e.g., $RO_2 + RO_2$ and $RO_2 + HO_2$) and SOA formation through them are also poorly understood despite the long-established generic mechanisms. Particularly, the major α-pinene SOA species observed in the atmosphere and laboratory studies may not be sufficiently explained by the existing hypotheses.[24-25] Therefore, it is of great importance to unravel these mechanistic puzzles as they are key to understanding α-pinene-derived SOA formation.

Many of the above-mentioned challenges are due to the complexity in the α-pinene ozonolysis system: immediately after the initial ozone addition, several isomeric $C_{10}H_{15}O_4$• are formed that undergo different routes at distinct rates and branching ratios. Elucidating such complexity may benefit from isolating specific reaction pathways, probing the key RO_2 species directly, and performing isomer-resolved compositional measurements. To this end, we synthesized two unsaturated carbonyl isomers ($C_{11}H_{18}O$ enone and enal), each capable of forming only one of the two CIs upon ozonolysis as produced by α-pinene (**Figure 1A**).[26-27] Namely, the CI_k with a terminal methyl ketone is formed by the enone (hereafter, CI_k-enone) and the CI_a with a terminal aldehyde is formed by the enal (hereafter, CI_a-enal). Ozonolysis experiments for the synthesized isomers were carried out, such that the two CI pathways could be separated in contrast to direct α-pinene ozonolysis. In these experiments, we used an iodide-adduct time-of-flight chemical ionization mass spectrometer (I-CIMS) to study the gas-phase closed-shell products and speciated RO_2 to provide kinetic insights into autoxidation and its competition with bimolecular reactions. In addition, isomer-resolved SOA compositions were measured using an ion-mobility

spectrometry time-of-flight mass spectrometer (IMS-TOF) to compare SOA formation from the two CI pathways.

Materials and Methods

Synthesis of CI_k-enone and CI_a-enal. CI_k-enone and CI_a-enal were synthesized based on schemes developed in-house. The complete synthesis procedures and characterization are provided in the **Supporting Information** (**SI, Text S1**). The ^{1}H and ^{13}C NMR and gas chromatograph – mass spectrometry with electron impact ionization (GC-EI-MS) (**Figure S1**) suggest that the purities of CI_k-enone and CI_a-enal are 97% and 95%, respectively. Possible impurities are volatile solvents used in the synthesis such as diethyl ether and hexanes. They are unlikely to affect the outcome of this work.

Laboratory experiments. Two sets of ozonolysis experiments of α-pinene (Sigma-Aldrich, 98%), CI_k-enone, and CI_a-enal were performed under 22 °C using two separate reactors (reactor schematics shown in **Figure S2** and experiments listed in **Tables S1–S2**). The laminar flowtube (Quartz, 110 cm long, 5.5 cm id., cone-shaped ends, volume ~ 2.1 L) was interfaced directly with the inlet of the ion-molecule reaction chamber of the I-CIMS without transfer tubing to measure the gas-phase composition. The CFSTR (cylindric stainless steel enclosure with interior Teflon coating, volume ~ 250 L) was operated under the dynamic mode with continuous injections of the reactants.[28] The flowtube's short residence time (t_R = 1 min) and "tubingless" design made it ideal to study the initially formed gas-phase products, including RO_2; the longer residence time in the CFSTR (t_R = 1 min) allows for investigation of the SOA formation. A zero-air generator (Aadco Instrument, Inc., 747–30) was used to supply clean dry air. The VOC was introduced into the reactors using a syringe pump. Methanol (Sigma-Aldrich, ≥ 99.9%) or cyclohexane (Sigma-

Aldrich, 99.5%) was introduced by a separate syringe pump as OH scavengers. O_3 was produced by an O_3 generator (Ozone Solutions Inc.) and measured by an O_3 analyzer (Thermo Environmental Instrument, Inc., 49C). The particle size distribution and number concentrations from the CFSTR experiments were measured by a scanning electric mobility sizer (SEMS) and mixing condensation particle counter (MCPC), respectively (Brechtel Inc.), from which the SOA mass concentrations were estimated at steady state, assuming the particle density of 1.2 g cm^{-3}.[29] Representative particle volume and size distribution data are shown in **Figure S3**.

Product analysis. The gas-phase products in the flowtube and CFSTR were measured in real time by the I-CIMS (Aerodyne Research Inc., m/Δm ~ 5000 at *m/Q* 300 Th) in most experiments.[30] For characterization purposes, in two CFSTR experiments with initial ~ 15 ppb of CI_k-enone and CI_a-enal, H_3O^+ was used as the reagent ion with CIMS (H_3O–CIMS, the same mass spectrometer as the I-CIMS), to detect CI_k-enone and CI_a-enal through proton transfer reactions, and to constrain their degradation kinetics upon ozonolysis (**Figure S4**). The "tubingless" flowtube configuration allows sensitive detection of the closed-shell oxygenated molecules as well as the hydroperoxyl radicals (HO_2) and speciated RO_2 (**Figures S5 and S6**). The I–CIMS measurements from the CFSTR experiments provides a complete picture of the gas-phase composition with longer timescale at steady state, shown by the representative mass spectra (*m/Q* 320 – 410 Th) in **Figure 2**. Consistent with prior studies, the I-CIMS mass spectrum of α-pinene ozonolysis gas-phase products (**Figure 2A**) are featured by dominant peaks of $C_{10}H_{14\text{-}16}O_{4\text{-}9}$.[19, 31] The mass spectra of the CI_k-enone (**Figure 2B**) and the CI_a-enal experiments (**Figure 2C**) exhibit the same characteristic pattern, suggesting that the two CI-initiated pathways dominate their ozonolysis products as well.

The SOA particles from the CFSTR experiments were collected by a sequential spot sampler (Aerosol Devices Inc.) downstream of a carbon denuder (removing organic vapors) at a flow rate of 1.6 L min^{-1} for 30 – 60 min. The collected particles were immediately extracted by 50 – 100 μL acetonitrile (Sigma-Aldrich, ≥ 99.9%), so that the organic concentration in the extracts were in the range of 10 – 100 μg mL^{-1}. The SOA samples were then characterized offline by the IMS-TOF with electrospray ionization (ESI) (Tofwerk Inc. and Aerodyne Research Inc., t/Δt ~ 100) through direct infusion or analyzed by the GC-EI-MS (Agilent Inc., 7890 GC and 5975 MSD) after derivatization (by additions of 25 μL N,O-Bis(trimethylsilyl)trifluoroacetamide (BSTFA) and 25 μL pyridine, both reagents from Sigma-Aldrich). Both analytical methods have been described in detail in our prior studies.[28, 32-36]

Kinetic modeling. The ozonolysis rates of CI_k-enone and CI_a-enal were found to be approximately 3.5 and 10 times slower than α-pinene ozonolysis, respectively (**Figure S4**); and thus, significantly higher O_3 concentrations than in the α-pinene experiments were needed to enhance VOC consumption. To ensure that the total $C_{10}H_{15}O_4$• production can be controlled to the same level between the two reactors and three VOCs such that the reaction kinetics and compositions of their products are comparable, a gas-phase kinetic model was built to guide the experiments. The model was based on the Master chemical mechanism (MCM v3.3.1),[37] with new branching ratios and yields of the initial ozonolysis of α-pinene,[21, 38] as well as CI_k-enone and CI_a-enal reactions (listed in **Table S3**). More details of the kinetic model can be found in the **SI text S2**. The model is mainly used to (1) constrain CI_k-enone and CI_a-enal oxidation kinetics; (2) estimate parent VOC consumption (for SOA yield calculations); (3) simulate net $C_{10}H_{15}O_4$• production ($P_{C10H15O4\bullet}$) such that results from the three VOCs can be compared:

$$P_{C10H15O4\bullet} = \int_0^t (k_{VOC+O3} \times [\mathrm{VOC}] \times [O_3] \times y_{CI} \times y_{VHP}) \quad (1)$$

where k_{VOC+O3} is the ozonolysis rate; y_{CI} and y_{VHP} are the yields of the C_{10}-CIs and the VHP intermediates, respectively (**Figure 1A**); and (4) constrain $C_{10}H_{15}O_4$• autoxidation rates between the two CI pathways based on published computational results (**see SI text S2**).[20-21]

Results and Discussion

Autoxidation vs. bimolecular RO_2 reactions (RO_2 + RO_2 and RO_2 + HO_2) in the ozonolysis of α-pinene, CI_k-enone, and CI_a-enal. The flowtube experiments span a range of initial O_3 concentrations with different OH scavengers (and thereby varying RO_2 and HO_2 concentrations). Thus, the RO_2 intermediates in these experiments could have distinct bimolecular lifetimes ($\tau_{bimolecular}$):

$$\tau_{bimolecular} = \frac{1}{k_{RO2+HO2} \times [HO2] + k_{RO2+RO2} \times [\Sigma RO2]} \qquad (2)$$

where $k_{RO2+HO2} = 2.2 \times 10^{-11}$ cm^3 molecule^{-1} s^{-1} under the experimental temperature based on MCM v3.3.1; $k_{RO2+RO2}$ is assumed to be 2.0×10^{-12} cm^3 molecule^{-1} s^{-1} between the C_{9-10} RO_2 species,[19] and 2.5×10^{-13} cm^3 molecule^{-1} s^{-1} for the cyclohexane-derived and other RO_2 species based on the MCM mechanism. HO_2 and RO_2 are estimated to be in the ranges of 6 – 110 ppt and 0.4 – 10 ppb, respectively. **Figure 3A** presents the estimated average $\tau_{bimolecular}$ under the studied α-pinene concentration as a function of initial O_3 using the kinetic model. Thus, the α-pinene flowtube experiments are expected to have $\tau_{bimolecular}$ of 2 – 20 s. In comparison, $\tau_{bimolecular}$ under typical atmospheric conditions are from 1 to >100 s,[39] suggested by previous field measurements;[6, 39-42] the calculated autoxidation lifetimes for the three cyclobutyl-ring-retained $C_{10}H_{15}O_4$• by Kurtén et al. are 7.1 s, 47.6 s, and 3.4 s (for a, b, and c in **Figure 1A**), respectively.[20] These comparisons suggest that under ambient conditions and the flowtube experiments in this work, the dynamic competition between autoxidation and bimolecular RO_2 pathways is always present.

The capability of speciated RO_2 measurements using the I-CIMS allows us to directly probe this competition. We focus on two major RO_2s: $C_{10}H_{15}O_4$• and $C_{10}H_{15}O_6$•. As illustrated in **Figure 1B**, $C_{10}H_{15}O_4$• could form $C_{10}H_{15}O_6$• through one step of autoxidation or two sequential $RO_2 + RO_2$ followed by alkoxy radical (RO) isomerization.[43] Given a typical branching ratio of 0.6 for RO formation from $RO_2 + RO_2$ and 0.5 for RO isomerization (**Table S3**), the yield of $C_{10}H_{15}O_6$• from $C_{10}H_{15}O_4$• through this pathway is only ~ 0.09. A fraction of $C_{10}H_{15}O_4$• can also be consumed by HO_2, making the yield of $C_{10}H_{15}O_6$• from $C_{10}H_{15}O_4$• through non-autoxidation pathways even smaller. To further minimize the contribution of the non-autoxidation pathways to $C_{10}H_{15}O_6$• formation, we specifically examined the conditions with relatively low O_3 concentrations and thus high $\tau_{bimolecular}$ (estimated to be > 5 s based on the kinetic model). **Figure 3B** presents the $C_{10}H_{15}O_6$• intensities in relation to $C_{10}H_{15}O_4$• bimolecular loss rate ($1/\tau_{bimolecular}$) under these conditions. As shown in **Figure 3B**, different linear relationships are observed for the three VOCs. Specifically, $C_{10}H_{15}O_6$• from CI_k-enone ozonolysis exhibit an approximately 20-fold higher yield than that from CI_a-enal ozonolysis at similar $C_{10}H_{15}O_4$• bimolecular loss rates, while $C_{10}H_{15}O_6$• from α-pinene ozonolysis lie between them. It should be mentioned that the differently structured $C_{10}H_{15}O_4$• could have different $RO_2 + RO_2$ rate constants, but as suggested by Zhao et al.,[19] the difference is likely small due to the similar α-pinene backbone. Sensitivity analysis was performed using the kinetic model to demonstrate that under the experimental conditions in **Figure 3B**, the contribution of the non-autoxidation pathways to $C_{10}H_{15}O_6$• remains significantly smaller than from autoxidation under a range of possible $RO_2 + RO_2$ rate constants (**Figure S7**). Therefore, the distinct yields of $C_{10}H_{15}O_6$• are most likely from different $C_{10}H_{15}O_4$• autoxidation rates: $C_{10}H_{15}O_4$• from CI_k-enone autoxidize much more rapidly than those from CI_a-enal (i.e., slope of 1.4 vs. 0.08).

It should also be noted that the ozonolysis of CI_k-enone and CI_a-enal might distribute different amounts of excess energy to the CIs in comparison to α-pinene ozonolysis, which, as reported by Iyer et al.,[21] could lead to somewhat different yields of the ring-opened $C_{10}H_{15}O_4$• from the VHP (30–80%, see **Figure 1A**). Nevertheless, the large difference between CI_k-enone and CI_a-enal shown in **Figure 3B** still clearly demonstrates that $C_{10}H_{15}O_4$• from CI_k-enone autoxidize much faster than those from CI_a-enal. To provide quantitative constraints on the $C_{10}H_{15}O_4$• autoxidation rates, we simulated the autoxidation rates from the CI_k-enone-derived $C_{10}H_{15}O_4$• relative to those from CI_a-enal (see **SI text S2**). We estimate that the CI_k-enone-derived $C_{10}H_{15}O_4$• have an averaged autoxidation rate on the order of 1 s^{-1} (**Figure S8**), which is about 20-fold higher than that from CI_a-enal estimated based on Kurtén et al. (~ 0.05 s^{-1}).[20] This is highly consistent with prior studies[4, 19] and the results shown in **Figure 3B**. Using the yield of the ring-opened $C_{10}H_{15}O_4$• from the VHP provided by Iyer et al.,[21] we further estimate that the ring-opened $C_{10}H_{15}O_4$• autoxidizes at ~ 1.2 – 2.7 s^{-1} (**Figure S8**). Note that the $C_{10}H_{15}O_6$• yields from α-pinene ozonolysis are closer to those from CI_a-enal ozonolysis in **Figure 3B**, suggesting that in α-pinene ozonolysis the fast autoxidizing $C_{10}H_{15}O_4$• (from CI_k) are likely in a smaller fraction while the majority of $C_{10}H_{15}O_4$• autoxidize slowly (from CI_a), consistent with prior work.[4, 19]

Further, we examined the major closed-shell products from the three VOCs. **Figure 3C–D** show the $C_{10}H_{14\text{-}16}O_x/C_{10}H_{14\text{-}16}O_4$ (x = 6, 7, 8, and 9) ratios as a function of $C_{10}H_{15}O_4$• production from the different experiments. In comparison to $C_{10}H_{14\text{-}16}O_4$ which can only be formed via $C_{10}H_{15}O_4$• bimolecular pathways, the $C_{10}H_{14\text{-}16}O_x/C_{10}H_{14\text{-}16}O_4$ (x = 6, 7, 8, and 9) ratios are expected to decrease with enhanced $C_{10}H_{15}O_4$• production if the $C_{10}H_{14\text{-}16}O_x$ are formed by autoxidation. In contrast, if the $C_{10}H_{14\text{-}16}O_x$ are formed via bimolecular pathways, their ratios to $C_{10}H_{14\text{-}16}O_4$ are expected to increase first as $RO_2 + RO_2$ starts to outrun $RO_2 + HO_2$. For $C_{10}H_{14\text{-}}$

$_{16}O_6$ and $C_{10}H_{14\text{-}16}O_7$ (**Figure 3C**), their ratios to $C_{10}H_{14\text{-}16}O_4$ from the CI_k-enone experiments indeed decrease with $C_{10}H_{15}O_4$• production, consistent with the autoxidation scheme. The same product ratios from the CI_a-enal experiments, however, exhibit the opposite trend, suggesting that these products are mostly formed from RO_2 bimolecular reactions. For the reference, these ratios from α-pinene ozonolysis stay fairly constant throughout the measurable range, implying a combination of the autoxidation and bimolecular pathways.

On the other hand, for the more oxidized $C_{10}H_{14\text{-}16}O_8$ and $C_{10}H_{14\text{-}16}O_9$ (**Figure 3D**), the trends of their ratios to $C_{10}H_{14\text{-}16}O_4$ more consistently agree with the autoxidation mechanisms for all three VOCs. However, these highly oxidized product ratios are on the same order of magnitude in the ozonolysis of α-pinene and CI_k-enone but are notably lower in the case for CI_a-enal. These results again demonstrate that autoxidation is less prominent in CI_a-enal ozonolysis. Additional functional groups were suggested to facilitate RO_2 autoxidation.[13] Thus, the least functionalized RO_2 in these systems, $C_{10}H_{15}O_4$• is most likely to be responsible for the large difference in autoxidation between the CI_k-enone and CI_a-enal experiments. Beyond the 1-min timescale in the flowtube experiments, the fates of RO_2 could be different; complex later-generation reactions could take place; partitioning to the particle phase could also affect the gas-phase compositions. Despite the additional complexity, some key observations in the gas phase are highly consistent between the CFSTR and the flowtube experiments. Particularly, the more oxidized products (i.e., $C_{10}H_{14\text{-}16}O_{8\text{-}9}$) from the CI_k-enone experiments are still more abundant than those from the CI_a-enal experiments (**Figure 2**). These measurements provide key experimental evidence in support of the recent computational work.[21] Our results suggest that a small fraction of $C_{10}H_{15}O_4$• (likely without the cyclobutyl ring) undergoes rapid autoxidation which could always outcompete

bimolecular reactions, while the majority of $C_{10}H_{15}O_4$• autoxidizes at much lower rates and could only compete with bimolecular reactions under high $\tau_{bimolecular}$ (e.g., > 20 s).

SOA formation and isomer-resolved compositions. The gas-phase measurements and analysis suggest that the two CI pathways from α-pinene ozonolysis produce different $C_{10}H_{15}O_4$• with distinct autoxidation rates. We further examined how the difference in gas-phase chemistry affects SOA formation and composition. From the CFSTR experiments, the steady-state SOA yields (= SOA mass/ΔVOC) were shown against the SOA mass concentrations (**Figure S9**). The SOA mass was not corrected for particle wall loss, but due to the similarity of the studied systems, the relative SOA yields should reflect the SOA formation potential of the three precursors. It appears that the overall SOA yields from ozonolysis of CI_k-enone and CI_a-enal are very similar to each other, both of which are approximately half of that from α-pinene ozonolysis. However, it should be noted that the yields of CI from CI_k-enone and CI_a-enal are 0.5 and 0.65, respectively (**Figure 1A**);[44] while that from α-pinene ozonolysis is 1.0. Therefore, we suggest that ozonolysis of CI_k-enone forms SOA at a slightly higher yield, which could likely be attributed to the above-mentioned higher autoxidation rates and hence HOM formation.

The SOA constituents from the CFSTR experiments were characterized by the isomer-resolved IMS-TOF technique. The IMS-TOF measurements characterize ionized molecules by their structure-dependent collisional cross sections, ion mobilities, and hence drift times in the IMS drift tube.[45] Thus, different drift times usually suggest different structures. In our previous studies, we have demonstrated that the IMS-TOF is able to clearly separate structural isomers.[28, 33, 35-36] Using the ESI in both the positive (+) and negative (–) ion modes allows for detections of the majority of the SOA constituents. An overview of the SOA molecular compositions is shown in **Figures S10–S11**.[46] **Figure 4A–B** illustrate the measured SOA from 20 ppb α-pinene ozonolysis

in the IMS drift time – *m/Q* diagrams in the (+)ESI and (–)ESI modes, respectively. In addition, the IMS-TOF driftgrams of two representative major SOA constituents are compared in **Figure 4C–D**: $C_{10}H_{16}O_5$ from the (+)ESI mode with sodium adduct and $C_9H_{14}O_4$ from the (–)ESI mode. Similar comparisons of many other major products ($C_{9\text{-}10}H_{14\text{-}16}O_{4\text{-}8}$) are presented in the **SI** (**Figures S12–S17**). Surprisingly, the majority of the large driftgram peaks in these comparisons align on identical drift times (precision better than ± 0.2 ms) for the SOA derived from α-pinene, CI_k-enone, and CI_a-enal, suggesting that the three VOCs' major SOA constituents have identical ion mobilities, and hence structures. The same type of analysis was carried out for a comprehensive list of formulas (**Figures S10–S11**) to examine the product overlaps among the three VOC systems. As shown in the Venn diagram in **Figure 4E**, we categorize the α-pinene ozonolysis SOA constituents into five groups: (*I*) products unique to α-pinene SOA; (*II*) products that are present only in α-pinene and CI_k-enone ozonolysis; (*III*) products that are present only in α-pinene and CI_a-enal ozonolysis; (*IV*) common products that are present in the SOA from all three VOCs; and (*V*) products that are present in the SOA from α-pinene ozonolysis and from the CI_k-enone + CI_a-enal mixtures (but not from CI_k-enone or CI_a-enal individually). Remarkably, an appreciable fraction of the α-pinene SOA constituents is "overlapped" with both the CI_k-enone and the CI_a-enal SOA (i.e., group *IV*). A quantitative presentation of this overlap is shown in **Figure 4F–G**, in which the peak number- and intensity-based fractions of the five groups are compared. At lower initial CI_k-enone and CI_a-enal concentrations (30 and 60 ppb), the overlap by all three types of SOA is unexpectedly high (40 – 50% by peak number and > 70% by peak intensity). In contrast, the α-pinene SOA constituents that are only produced when the CI_k-enone and the CI_a-enal co-exist in the same experiments (i.e., group *V*) are always below 10%. Note that despite the substantial overlap between the three SOA compositions, the detailed isomer intensities are usually

different (exemplified by **Figures S12–S17**), implying that the common products are not formed at the same yields between the two CI pathways. Unfortunately, it is impossible to identify unique SOA constituents associated with the autoxidation pathways without knowing their structures.

The fact that group *IV* always has larger fractions by peak intensity than by peak number, while group *I* is the opposite suggest that the overlapped constituents are usually major products. As the initial VOC concentrations increase to 300 ppb and 1000 ppb, the summed fractions of the overlapped groups (i.e., *II – V*) decrease. The majority of this decrease is from the reduction in group *IV*, while the groups *II* and *III* remain unchanged or even slightly increase. From another viewpoint using the CI_k-enone or CI_a-enal SOA as the base (**Figure 4** uses α-pinene SOA as the base), the fractions of the common products decreased with increased initial VOC concentrations (**Figure S18**). These phenomena clearly demonstrate the "splitting" of the overlapped SOA formed from CI_k-enone and CI_a-enal as the VOC concentrations increase. The fractions of the common products in **Figure S18** are large (> 0.8) at low VOC concentrations, suggesting that major fractions of CI_k-enone and CI_a-enal oxidation undergo unrecognized pathways, leading to the mutual products. These results also suggest that the potential different energy distributions during ozonolysis of CI_k-enone and CI_a-enal do not appreciably form new products than α-pinene ozonolysis. With enhanced VOC concentrations, it is expected that bimolecular SCI chemistry (i.e., SCI reacting with carboxylic acids and carbonyls) become more important;[38] the reduced effectiveness of OH scavenger could also lead to higher branching ratios of OH-oxidation. These "high-concentration-favored" pathways more likely form products with different structures between CI_k-enone and CI_a-enal. Thus, the common products are suggested to stem from nontraditional CI–initiated pathways. This hypothesis is further evidenced by the formation of pinic acid, a major α-pinene SOA product. From the IMS-TOF and GC-MS measurements, pinic

304 acid was observed in both the CI_k-enone and CI_a-enal experiments under lower VOC
305 concentrations (**Figures 4D and S19**). Under higher VOC concentrations, pinic acid was only
306 largely present in the CI_a-enal experiments, but not in the CI_k-enone SOA (**Figure S17**). From the
307 reaction mechanism that is currently understood, the formation of pinic acid should only be
308 expected from one $C_{10}H_{15}O_4$• isomer by CI_a-enal ozonolysis (**Figure S20**).[47] Therefore, we suggest
309 that an unrecognized pathway (or pathways) must exist from CI_k-enone to the CI_a-enal-derived
310 intermediates and hence pinic acid. This pathway is especially pronounced under lower VOC
311 concentrations, which is more relevant to the real atmosphere. Elucidation of this pathway(s) is
312 crucial because pinic acid is often found to be one of the largest organic compounds in atmospheric
313 fine particles.[6, 48-51]

314 **Possible mechanisms and implications for atmospheric chemistry.** In this study, the
315 gas-phase measurements combining with the SOA compositional analysis suggest that the two CI
316 pathways from α-pinene ozonolysis initially produce different $C_{10}H_{15}O_4$• isomers that undergo
317 further reactions to, however, form products mostly with the same structures. Such common
318 products are enhanced under lower VOC concentrations, suggesting that certain bimolecular
319 reactions inhibit their formation. This also indicates that these common products might originate
320 from unimolecular pathways. Such bimolecular-unimolecular competition may be present in two
321 mechanisms: (1) RO_2 pathways (**Figure 1B**) and (2) SCI pathways (**Figures S20–S21**). For the
322 RO_2 pathways, however, we are not aware of any mechanisms that could largely lead to the same
323 products from initially different RO_2 without fragmentation. On the other hand, the SCI from α-
324 pinene ozonolysis was suggested to quickly undergo unimolecular reactions (**Figure S21**) to form
325 VHP in the same way as the excited CI;[12, 52] or form secondary ozonide (SOZ).[53-55] Alternatively,
326 there was also evidence for bimolecular reactions of the SCI.[19, 52, 56-57] To explain the IMS-TOF

observations, at least one of the unimolecular pathways from one SCI has to produce $C_{10}H_{15}O_4$• identical to those from the other CI pathway. A hypothetical mechanism is provided that describes unimolecular H-shifts of the SCI to form these $C_{10}H_{15}O_4$• isomers (**Figure S20**). These "long-range" H-shifts appear to be unfavored by the strained cyclobutyl ring, but similar mechanisms have been proposed in prior studies to explain the formation of pinonic acid and pinic acid.[24, 27] Another plausible mechanism derived from the SOZ was also shown (**Figure S22**) to form the $C_{10}H_{15}O_4$• that leads to pinic acid.[58] But if this is indeed the mechanism for our observation, it is possible that the lower energy distributed to the CIs in the ozonolysis of CI_k-enone and CI_a-enal than actual α-pinene ozonolysis could have overestimated the fraction of common products between the two CI pathways. It should be clearly stressed again that these tentative mechanisms are only hypothetical to explain the IMS-TOF observations. Despite some evidence for their occurrence,[24, 27, 58] direct support or contradiction from computational and experimental studies are required. With these possible mechanisms, both CI pathways could lead to the three $C_{10}H_{15}O_4$• isomers with the cyclobutyl ring intact, but likely at different branching ratios. This could explain the common SOA constituents measured by the IMS-TOF. However, the ring-opened $C_{10}H_{15}O_4$• isomer (**Figure 1A**) may only be formed from the CI_k pathway,[21] consistent with the faster autoxidation rate measured by the I-CIMS.

This work provides new insights into α-pinene ozonolysis mechanisms through isolating the two CI pathways, directly probing gas-phase RO_2, and performing isomer-resolved SOA compositional analysis. The results suggest that both CI pathways likely form the same $C_{10}H_{15}O_4$• isomers with the cyclobutyl ring intact which autoxidize relatively slowly. In addition, CI_k could produce a ring-opened $C_{10}H_{15}O_4$• that autoxidizes much more rapidly. The rapid $C_{10}H_{15}O_4$• autoxidation leads to higher HOM yields and thus higher SOA formation through the CI_k channel.

But both CI pathways form mostly common products since the majority of the initial $C_{10}H_{15}O_4$• isomers are identical. These new mechanistic insights are likely sensitive to VOC concentrations from ambient-relevant to laboratory conditions. The rapid ring-opened $C_{10}H_{15}O_4$• autoxidation should always outcompete bimolecular reactions, while the ring-intact $C_{10}H_{15}O_4$• autoxidation is much less pronounced under typical laboratory conditions. The two CI channels lead to more common products when VOC concentrations are lower. These implications highlight the importance of considering new mechanisms in atmospheric models and interpreting ambient-measured SOA species (e.g., pinic acid). Despite of the reported observations, the exact mechanisms and kinetics are still not well understood or constrained. Future computational and experimental studies to examine the hypothesized mechanisms are needed for a more complete understanding of these important atmospheric processes.

Associated Contents

Supporting Information

Detailed description of the kinetic model and supplementary analysis results are provided in the Supporting Information.

Author Information

Corresponding Author

*E-mail: haofei.zhang@ucr.edu

Notes

The authors declare no competing financial interest.

Acknowledgements

The work was supported by the start-up funding granted to H.Z. by University of California, Riverside. The chemical analysis was partially supported by National Science Foundation (CHE-2002413 and AGS-1953905). We thank useful discussions with Theo Kurtén (University of Helsinki), Siddharth Iyer (Tempere University), Bo Long (Guizhou Minzu University), and Lu Xu (Caltech).

References

1. Criegee, R., Mechanism of Ozonolysis. *Angewandte Chemie International Edition in English* **1975,** *14* (11), 745-752.
2. Lelieveld, J.; Butler, T. M.; Crowley, J. N.; Dillon, T. J.; Fischer, H.; Ganzeveld, L.; Harder, H.; Lawrence, M. G.; Martinez, M.; Taraborrelli, D.; Williams, J., Atmospheric Oxidation Capacity Sustained by a Tropical Forest. *Nature* **2008,** *452*, 737.
3. Lelieveld, J.; Gromov, S.; Pozzer, A.; Taraborrelli, D., Global Tropospheric Hydroxyl Distribution, Budget and Reactivity. *Atmos. Chem. Phys.* **2016,** *16* (19), 12477-12493.
4. Ehn, M.; Thornton, J. A.; Kleist, E.; Sipila, M.; Junninen, H.; Pullinen, I.; Springer, M.; Rubach, F.; Tillmann, R.; Lee, B.; Lopez-Hilfiker, F.; Andres, S.; Acir, I.-H.; Rissanen, M.; Jokinen, T.; Schobesberger, S.; Kangasluoma, J.; Kontkanen, J.; Nieminen, T.; Kurten, T.; Nielsen, L. B.; Jorgensen, S.; Kjaergaard, H. G.; Canagaratna, M.; Maso, M. D.; Berndt, T.; Petaja, T.; Wahner, A.; Kerminen, V.-M.; Kulmala, M.; Worsnop, D. R.; Wildt, J.; Mentel, T. F., A Large Source of Low-Volatility Secondary Organic Aerosol. *Nature* **2014,** *506* (7489), 476-479.
5. Johnson, D.; Marston, G., The Gas-Phase Ozonolysis of Unsaturated Volatile Organic Compounds in the Troposphere. *Chem. Soc. Rev.* **2008,** *37* (4), 699-716.
6. Zhang, H.; Yee, L. D.; Lee, B. H.; Curtis, M. P.; Worton, D. R.; Isaacman-VanWertz, G.; Offenberg, J. H.; Lewandowski, M.; Kleindienst, T. E.; Beaver, M. R.; Holder, A. L.; Lonneman, W. A.; Docherty, K. S.; Jaoui, M.; Pye, H. O. T.; Hu, W.; Day, D. A.; Campuzano-Jost, P.; Jimenez, J. L.; Guo, H.; Weber, R. J.; de Gouw, J.; Koss, A. R.; Edgerton, E. S.; Brune, W.; Mohr, C.; Lopez-Hilfiker, F. D.; Lutz, A.; Kreisberg, N. M.; Spielman, S. R.; Hering, S. V.; Wilson, K. R.; Thornton, J. A.; Goldstein, A. H., Monoterpenes Are the Largest Source of Summertime Organic Aerosol in the Southeastern United States. *Proc. Natl. Acad. Sci. U.S.A.* **2018,** *115* (9), 2038.
7. Guenther, A.; Hewitt, C. N.; Erickson, D.; Fall, R.; Geron, C.; Graedel, T.; Harley, P.; Klinger, L.; Lerdau, M.; McKay, W. A.; Pierce, T.; Scholes, B.; Steinbrecher, R.; Tallamraju, R.; Taylor, J.; Zimmerman, P., A Global Model of Natural Volatile Organic Compound Emissions. *J. Geophys. Res. Atmos.* **1995,** *100* (D5), 8873-8892.
8. Atkinson, R.; Aschmann, S. M.; Arey, J.; Shorees, B., Formation of OH Radicals in the Gas Phase Reactions of O3 with a Series of Terpenes. *J. Geophys. Res. Atmos.* **1992,** *97* (D5), 6065-6073.
9. Aschmann, S. M.; Arey, J.; Atkinson, R., OH Radical Formation from the Gas-Phase Reactions of O3 with a Series of Terpenes. *Atmos. Environ.* **2002,** *36* (27), 4347-4355.
10. Paulson, S. E.; Chung, M.; Sen, A. D.; Orzechowska, G., Measurement of OH Radical Formation from the Reaction of Ozone with Several Biogenic Alkenes. *J. Geophys. Res. Atmos.* **1998,** *103* (D19), 25533-25539.
11. Zhang, D.; Zhang, R., Ozonolysis of α-Pinene and β-Pinene: Kinetics and Mechanism. *J. Chem. Phys.* **2005,** *122* (11), 114308.
12. Vereecken, L.; Novelli, A.; Taraborrelli, D., Unimolecular Decay Strongly Limits the Atmospheric Impact of Criegee Intermediates. *Phys. Chem. Chem. Phys.* **2017,** *19* (47), 31599-31612.
13. Crounse, J. D.; Nielsen, L. B.; Jørgensen, S.; Kjaergaard, H. G.; Wennberg, P. O., Autoxidation of Organic Compounds in the Atmosphere. *J. Phys. Chem. Lett.* **2013,** *4* (20), 3513-3520.

14. Bianchi, F.; Kurtén, T.; Riva, M.; Mohr, C.; Rissanen, M. P.; Roldin, P.; Berndt, T.; Crounse, J. D.; Wennberg, P. O.; Mentel, T. F.; Wildt, J.; Junninen, H.; Jokinen, T.; Kulmala, M.; Worsnop, D. R.; Thornton, J. A.; Donahue, N.; Kjaergaard, H. G.; Ehn, M., Highly Oxygenated Organic Molecules (Hom) from Gas-Phase Autoxidation Involving Peroxy Radicals: A Key Contributor to Atmospheric Aerosol. *Chem. Rev.* **2019,** *119* (6), 3472-3509.
15. Atkinson, R., Gas-Phase Tropospheric Chemistry of Organic Compounds: A Review. *Atmos. Environ.* **2007,** *41*, 200-240.
16. Tröstl, J.; Chuang, W. K.; Gordon, H.; Heinritzi, M.; Yan, C.; Molteni, U.; Ahlm, L.; Frege, C.; Bianchi, F.; Wagner, R.; Simon, M.; Lehtipalo, K.; Williamson, C.; Craven, J. S.; Duplissy, J.; Adamov, A.; Almeida, J.; Bernhammer, A.-K.; Breitenlechner, M.; Brilke, S.; Dias, A.; Ehrhart, S.; Flagan, R. C.; Franchin, A.; Fuchs, C.; Guida, R.; Gysel, M.; Hansel, A.; Hoyle, C. R.; Jokinen, T.; Junninen, H.; Kangasluoma, J.; Keskinen, H.; Kim, J.; Krapf, M.; Kürten, A.; Laaksonen, A.; Lawler, M.; Leiminger, M.; Mathot, S.; Möhler, O.; Nieminen, T.; Onnela, A.; Petäjä, T.; Piel, F. M.; Miettinen, P.; Rissanen, M. P.; Rondo, L.; Sarnela, N.; Schobesberger, S.; Sengupta, K.; Sipilä, M.; Smith, J. N.; Steiner, G.; Tomè, A.; Virtanen, A.; Wagner, A. C.; Weingartner, E.; Wimmer, D.; Winkler, P. M.; Ye, P.; Carslaw, K. S.; Curtius, J.; Dommen, J.; Kirkby, J.; Kulmala, M.; Riipinen, I.; Worsnop, D. R.; Donahue, N. M.; Baltensperger, U., The Role of Low-Volatility Organic Compounds in Initial Particle Growth in the Atmosphere. *Nature* **2016,** *533* (7604), 527-531.
17. Kirkby, J.; Duplissy, J.; Sengupta, K.; Frege, C.; Gordon, H.; Williamson, C.; Heinritzi, M.; Simon, M.; Yan, C.; Almeida, J.; Tröstl, J.; Nieminen, T.; Ortega, I. K.; Wagner, R.; Adamov, A.; Amorim, A.; Bernhammer, A.-K.; Bianchi, F.; Breitenlechner, M.; Brilke, S.; Chen, X.; Craven, J.; Dias, A.; Ehrhart, S.; Flagan, R. C.; Franchin, A.; Fuchs, C.; Guida, R.; Hakala, J.; Hoyle, C. R.; Jokinen, T.; Junninen, H.; Kangasluoma, J.; Kim, J.; Krapf, M.; Kürten, A.; Laaksonen, A.; Lehtipalo, K.; Makhmutov, V.; Mathot, S.; Molteni, U.; Onnela, A.; Peräkylä, O.; Piel, F.; Petäjä, T.; Praplan, A. P.; Pringle, K.; Rap, A.; Richards, N. A. D.; Riipinen, I.; Rissanen, M. P.; Rondo, L.; Sarnela, N.; Schobesberger, S.; Scott, C. E.; Seinfeld, J. H.; Sipilä, M.; Steiner, G.; Stozhkov, Y.; Stratmann, F.; Tomé, A.; Virtanen, A.; Vogel, A. L.; Wagner, A. C.; Wagner, P. E.; Weingartner, E.; Wimmer, D.; Winkler, P. M.; Ye, P.; Zhang, X.; Hansel, A.; Dommen, J.; Donahue, N. M.; Worsnop, D. R.; Baltensperger, U.; Kulmala, M.; Carslaw, K. S.; Curtius, J., Ion-Induced Nucleation of Pure Biogenic Particles. *Nature* **2016,** *533* (7604), 521-526.
18. Bianchi, F.; Tröstl, J.; Junninen, H.; Frege, C.; Henne, S.; Hoyle, C. R.; Molteni, U.; Herrmann, E.; Adamov, A.; Bukowiecki, N.; Chen, X.; Duplissy, J.; Gysel, M.; Hutterli, M.; Kangasluoma, J.; Kontkanen, J.; Kürten, A.; Manninen, H. E.; Münch, S.; Peräkylä, O.; Petäjä, T.; Rondo, L.; Williamson, C.; Weingartner, E.; Curtius, J.; Worsnop, D. R.; Kulmala, M.; Dommen, J.; Baltensperger, U., New Particle Formation in the Free Troposphere: A Question of Chemistry and Timing. *Science* **2016,** *352* (6289), 1109.
19. Zhao, Y.; Thornton, J. A.; Pye, H. O. T., Quantitative Constraints on Autoxidation and Dimer Formation from Direct Probing of Monoterpene-Derived Peroxy Radical Chemistry. *Proc. Natl. Acad. Sci. U.S.A.* **2018,** *115* (48), 12142.
20. Kurtén, T.; Rissanen, M. P.; Mackeprang, K.; Thornton, J. A.; Hyttinen, N.; Jørgensen, S.; Ehn, M.; Kjaergaard, H. G., Computational Study of Hydrogen Shifts and Ring-Opening Mechanisms in α-Pinene Ozonolysis Products. *J. Phys. Chem. A* **2015,** *119* (46), 11366-11375.
21. Iyer, S.; Rissanen, M. P.; Valiev, R.; Barua, S.; Krechmer, J. E.; Thornton, J.; Ehn, M.; Kurtén, T., Molecular Mechanism for Rapid Autoxidation in α-Pinene Ozonolysis. *Nat. Comm.* **2021,** *12* (1), 878.

22. Roldin, P.; Ehn, M.; Kurtén, T.; Olenius, T.; Rissanen, M. P.; Sarnela, N.; Elm, J.; Rantala, P.; Hao, L.; Hyttinen, N.; Heikkinen, L.; Worsnop, D. R.; Pichelstorfer, L.; Xavier, C.; Clusius, P.; Öström, E.; Petäjä, T.; Kulmala, M.; Vehkamäki, H.; Virtanen, A.; Riipinen, I.; Boy, M., The Role of Highly Oxygenated Organic Molecules in the Boreal Aerosol-Cloud-Climate System. *Nat. Comm.* **2019,** *10* (1), 4370.
23. Weber, J.; Archer-Nicholls, S.; Griffiths, P.; Berndt, T.; Jenkin, M.; Gordon, H.; Knote, C.; Archibald, A. T., Cri-Hom: A Novel Chemical Mechanism for Simulating Highly Oxygenated Organic Molecules (Homs) in Global Chemistry–Aerosol–Climate Models. *Atmos. Chem. Phys.* **2020,** *20* (18), 10889-10910.
24. Jenkin, M. E.; Shallcross, D. E.; Harvey, J. N., Development and Application of a Possible Mechanism for the Generation of Cis-Pinic Acid from the Ozonolysis of Alpha- and Beta-Pinene. *Atmos. Environ.* **2000,** *34* (18), 2837-2850.
25. Zhang, X.; McVay, R. C.; Huang, D. D.; Dalleska, N. F.; Aumont, B.; Flagan, R. C.; Seinfeld, J. H., Formation and Evolution of Molecular Products in α-Pinene Secondary Organic Aerosol. *Proc. Natl. Acad. Sci. U.S.A.* **2015,** *112* (46), 14168-14173.
26. Ma, Y.; Luciani, T.; Porter, R. A.; Russell, A. T.; Johnson, D.; Marston, G., Organic Acid Formation in the Gas-Phase Ozonolysis of α-Pinene. *Phys. Chem. Chem. Phys.* **2007,** *9* (37), 5084-5087.
27. Ma, Y.; Willcox, T. R.; Russell, A. T.; Marston, G., Pinic and Pinonic Acid Formation in the Reaction of Ozone with α-Pinene. *Chemical Communications* **2007,** (13), 1328-1330.
28. Mayorga, R. J.; Zhao, Z.; Zhang, H., Formation of Secondary Organic Aerosol from Nitrate Radical Oxidation of Phenolic VOCs: Implications for Nitration Mechanisms and Brown Carbon Formation. *Atmos. Environ.* **2021,** *244*, 117910.
29. Kostenidou, E.; Pathak, R. K.; Pandis, S. N., An Algorithm for the Calculation of Secondary Organic Aerosol Density Combining Ams and Smps Data. *Aerosol Sci. Technol.* **2007,** *41* (11), 1002-1010.
30. Lee, B. H.; Lopez-Hilfiker, F. D.; Mohr, C.; Kurtén, T.; Worsnop, D. R.; Thornton, J. A., An Iodide-Adduct High-Resolution Time-of-Flight Chemical-Ionization Mass Spectrometer: Application to Atmospheric Inorganic and Organic Compounds. *Environ. Sci. Technol.* **2014,** *48* (11), 6309-6317.
31. Zhang, X.; Lambe, A. T.; Upshur, M. A.; Brooks, W. A.; Gray Bé, A.; Thomson, R. J.; Geiger, F. M.; Surratt, J. D.; Zhang, Z.; Gold, A.; Graf, S.; Cubison, M. J.; Groessl, M.; Jayne, J. T.; Worsnop, D. R.; Canagaratna, M. R., Highly Oxygenated Multifunctional Compounds in α-Pinene Secondary Organic Aerosol. *Environ. Sci. Technol.* **2017,** *51* (11), 5932-5940.
32. Zhao, Z.; Le, C.; Xu, Q.; Peng, W.; Jiang, H.; Lin, Y.-H.; Cocker, D. R.; Zhang, H., Compositional Evolution of Secondary Organic Aerosol as Temperature and Relative Humidity Cycle in Atmospherically Relevant Ranges. *ACS Earth Space Chem.* **2019,** *3* (11), 2549-2558.
33. Zhao, Z.; Tolentino, R.; Lee, J.; Vuong, A.; Yang, X.; Zhang, H., Interfacial Dimerization by Organic Radical Reactions During Heterogeneous Oxidative Aging of Oxygenated Organic Aerosols. *J. Phys. Chem. A* **2019,** *123* (50), 10782-10792.
34. Zhao, Z.; Xu, Q.; Yang, X.; Zhang, H., Heterogeneous Ozonolysis of Endocyclic Unsaturated Organic Aerosol Proxies: Implications for Criegee Intermediate Dynamics and Later-Generation Reactions. *ACS Earth Space Chem.* **2019,** *3* (3), 344-356.
35. Zhao, Z.; Yang, X.; Lee, J.; Tolentino, R.; Mayorga, R.; Zhang, W.; Zhang, H., Diverse Reactions in Highly Functionalized Organic Aerosols During Thermal Desorption. *ACS Earth Space Chem.* **2020,** *4* (2), 283-296.

514 36. Zhao, Z.; Mayorga, R.; Lee, J.; Yang, X.; Tolentino, R.; Zhang, W.; Vuong, A.; Zhang, H.,
515 Site-Specific Mechanisms in OH-Initiated Organic Aerosol Heterogeneous Oxidation Revealed
516 by Isomer-Resolved Molecular Characterization. *ACS Earth Space Chem.* **2020,** *4* (5), 783-794.
517 37. Saunders, S. M.; Jenkin, M. E.; Derwent, R. G.; Pilling, M. J., Protocol for the
518 Development of the Master Chemical Mechanism, MCM v3 (Part A): Tropospheric Degradation
519 of Non-Aromatic Volatile Organic Compounds. *Atmos. Chem. Phys.* **2003,** *3* (1), 161-180.
520 38. Claflin, M. S.; Krechmer, J. E.; Hu, W.; Jimenez, J. L.; Ziemann, P. J., Functional Group
521 Composition of Secondary Organic Aerosol Formed from Ozonolysis of α-Pinene under High
522 VOC and Autoxidation Conditions. *ACS Earth Space Chem.* **2018,** *2* (11), 1196–1210.
523 39. Praske, E.; Otkjær, R. V.; Crounse, J. D.; Hethcox, J. C.; Stoltz, B. M.; Kjaergaard, H. G.;
524 Wennberg, P. O., Atmospheric Autoxidation Is Increasingly Important in Urban and Suburban
525 North America. *Proc. Natl. Acad. Sci. U.S.A.* **2018,** *115* (1), 64.
526 40. Ryerson, T. B.; Andrews, A. E.; Angevine, W. M.; Bates, T. S.; Brock, C. A.; Cairns, B.;
527 Cohen, R. C.; Cooper, O. R.; de Gouw, J. A.; Fehsenfeld, F. C.; Ferrare, R. A.; Fischer, M. L.;
528 Flagan, R. C.; Goldstein, A. H.; Hair, J. W.; Hardesty, R. M.; Hostetler, C. A.; Jimenez, J. L.;
529 Langford, A. O.; McCauley, E.; McKeen, S. A.; Molina, L. T.; Nenes, A.; Oltmans, S. J.; Parrish,
530 D. D.; Pederson, J. R.; Pierce, R. B.; Prather, K.; Quinn, P. K.; Seinfeld, J. H.; Senff, C. J.;
531 Sorooshian, A.; Stutz, J.; Surratt, J. D.; Trainer, M.; Volkamer, R.; Williams, E. J.; Wofsy, S. C.,
532 The 2010 California Research at the Nexus of Air Quality and Climate Change (CalNex) Field
533 Study. *J. Geophys. Res. Atmos.* **2013,** *118* (11), 5830-5866.
534 41. Martin, S. T.; Artaxo, P.; Machado, L. A. T.; Manzi, A. O.; Souza, R. A. F.; Schumacher,
535 C.; Wang, J.; Andreae, M. O.; Barbosa, H. M. J.; Fan, J.; Fisch, G.; Goldstein, A. H.; Guenther,
536 A.; Jimenez, J. L.; Pöschl, U.; Silva Dias, M. A.; Smith, J. N.; Wendisch, M., Introduction:
537 Observations and Modeling of the Green Ocean Amazon (Goamazon2014/5). *Atmos. Chem. Phys.*
538 **2016,** *16* (8), 4785-4797.
539 42. Vasquez, K. T.; Allen, H. M.; Crounse, J. D.; Praske, E.; Xu, L.; Noelscher, A. C.;
540 Wennberg, P. O., Low-Pressure Gas Chromatography with Chemical Ionization Mass
541 Spectrometry for Quantification of Multifunctional Organic Compounds in the Atmosphere.
542 *Atmos. Meas. Tech.* **2018,** *11* (12), 6815-6832.
543 43. Atkinson, R., Atmospheric Reactions of Alkoxy and β-Hydroxyalkoxy Radicals. *Int. J.*
544 *Chem. Kinet.* **1997,** *29* (2), 99-111.
545 44. Atkinson, R., Gas-Phase Tropospheric Chemistry of Volatile Organic Compounds: 1.
546 Alkanes and Alkenes. *J. Phys. Chem. Ref. Data* **1997,** *26* (2), 215-290.
547 45. Zhang, X.; Krechmer, J. E.; Groessl, M.; Xu, W.; Graf, S.; Cubison, M.; Jayne, J. T.;
548 Jimenez, J. L.; Worsnop, D. R.; Canagaratna, M. R., A Novel Framework for Molecular
549 Characterization of Atmospherically Relevant Organic Compounds Based on Collision Cross
550 Section and Mass-to-Charge Ratio. *Atmos. Chem. Phys.* **2016,** *16* (20), 12945-12959.
551 46. Nguyen, T. B.; Roach, P. J.; Laskin, J.; Laskin, A.; Nizkorodov, S. A., Effect of Humidity
552 on the Composition of Isoprene Photooxidation Secondary Organic Aerosol. *Atmos. Chem. Phys.*
553 **2011,** *11* (14), 6931-6944.
554 47. E. Jenkin, M.; Shallcross, D. E.; Harvey, J. N., Development and Application of a Possible
555 Mechanism for the Generation of Cis-Pinic Acid from the Ozonolysis of α- and β-Pinene. *Atmos.*
556 *Environ.* **2000,** *34* (18), 2837-2850.
557 48. Kavouras, I. G.; Mihalopoulos, N.; Stephanou, E. G., Formation of Atmospheric Particles
558 from Organic Acids Produced by Forests. *Nature* **1998,** *395* (6703), 683-686.

559 49. Yu, J.; Griffin, R. J.; Cocker Iii, D. R.; Flagan, R. C.; Seinfeld, J. H.; Blanchard, P.,
560 Observation of Gaseous and Particulate Products of Monoterpene Oxidation in Forest
561 Atmospheres. *Geophys. Res. Lett.* **1999,** *26* (8), 1145-1148.
562 50. Boy, M.; Petäjä, T.; Dal Maso, M.; Rannik, Ü.; Rinne, J.; Aalto, P.; Laaksonen, A.;
563 Vaattovaara, P.; Joutsensaari, J.; Hoffmann, T.; Warnke, J.; Apostolaki, M.; Stephanou, E. G.;
564 Tsapakis, M.; Kouvarakis, A.; Pio, C.; Carvalho, A.; Römpp, A.; Moortgat, G.; Spirig, C.;
565 Guenther, A.; Greenberg, J.; Ciccioli, P.; Kulmala, M., Overview of the Field Measurement
566 Campaign in Hyytiälä, August 2001 in the Framework of the Eu Project Osoa. *Atmos. Chem. Phys.*
567 **2004,** *4* (3), 657-678.
568 51. Claeys, M.; Szmigielski, R.; Vermeylen, R.; Wang, W.; Shalamzari, M. S.; Maenhaut, W.
569 In *Tracers for Biogenic Secondary Organic Aerosol from α-Pinene and Related Monoterpenes:*
570 *An Overview*, NATO Science for Peace and Security Series C-Environmental Security, Dordrecht,
571 Netherlands, Rudziński, I. B. a. K. J., Ed. Dordrecht, Netherlands, 2013; pp 227–238.
572 52. Newland, M. J.; Rickard, A. R.; Sherwen, T.; Evans, M. J.; Vereecken, L.; Muñoz, A.;
573 Ródenas, M.; Bloss, W. J., The Atmospheric Impacts of Monoterpene Ozonolysis on Global
574 Stabilised Criegee Intermediate Budgets and SO2 Oxidation: Experiment, Theory and Modelling.
575 *Atmos. Chem. Phys.* **2018,** *18* (8), 6095-6120.
576 53. Donahue, N. M.; Huff Hartz, K. E.; Chuong, B.; Presto, A. A.; Stanier, C. O.; Rosenhørn,
577 T.; Robinson, A. L.; Pandis, S. N., Critical Factors Determining the Variation in SOA Yields from
578 Terpene Ozonolysis: A Combined Experimental and Computational Study. *Faraday Discuss.*
579 **2005,** *130* (0), 295-309.
580 54. Long, B.; Bao, J. L.; Truhlar, D. G., Rapid Unimolecular Reaction of Stabilized Criegee
581 Intermediates and Implications for Atmospheric Chemistry. *Nat. Comm.* **2019,** *10* (1), 2003.
582 55. Bagchi, A.; Yu, Y.; Huang, J.-H.; Tsai, C.-C.; Hu, W.-P.; Wang, C. C., Evidence and
583 Evolution of Criegee Intermediates, Hydroperoxides and Secondary Organic Aerosols Formed via
584 Ozonolysis of α-Pinene. *Phys. Chem. Chem. Phys.* **2020,** *22* (12), 6528-6537.
585 56. Docherty, K. S.; Ziemann, P. J., Effects of Stabilized Criegee Intermediate and OH Radical
586 Scavengers on Aerosol Formation from Reactions of β-Pinene with O 3. *Aerosol Sci. Technol.*
587 **2003,** *37* (11), 877-891.
588 57. Kristensen, K.; Watne, Å. K.; Hammes, J.; Lutz, A.; Petäjä, T.; Hallquist, M.; Bilde, M.;
589 Glasius, M., High-Molecular Weight Dimer Esters Are Major Products in Aerosols from α-Pinene
590 Ozonolysis and the Boreal Forest. *Environ. Sci. Technol. Lett.* **2016,** *3* (8), 280-285.
591 58. Ellis, S. R.; Pham, H. T.; in het Panhuis, M.; Trevitt, A. J.; Mitchell, T. W.; Blanksby, S.
592 J., Radical Generation from the Gas-Phase Activation of Ionized Lipid Ozonides. *J. Am. Soc. Mass*
593 *Spectrom.* **2017,** *28* (7), 1345-1358.
594

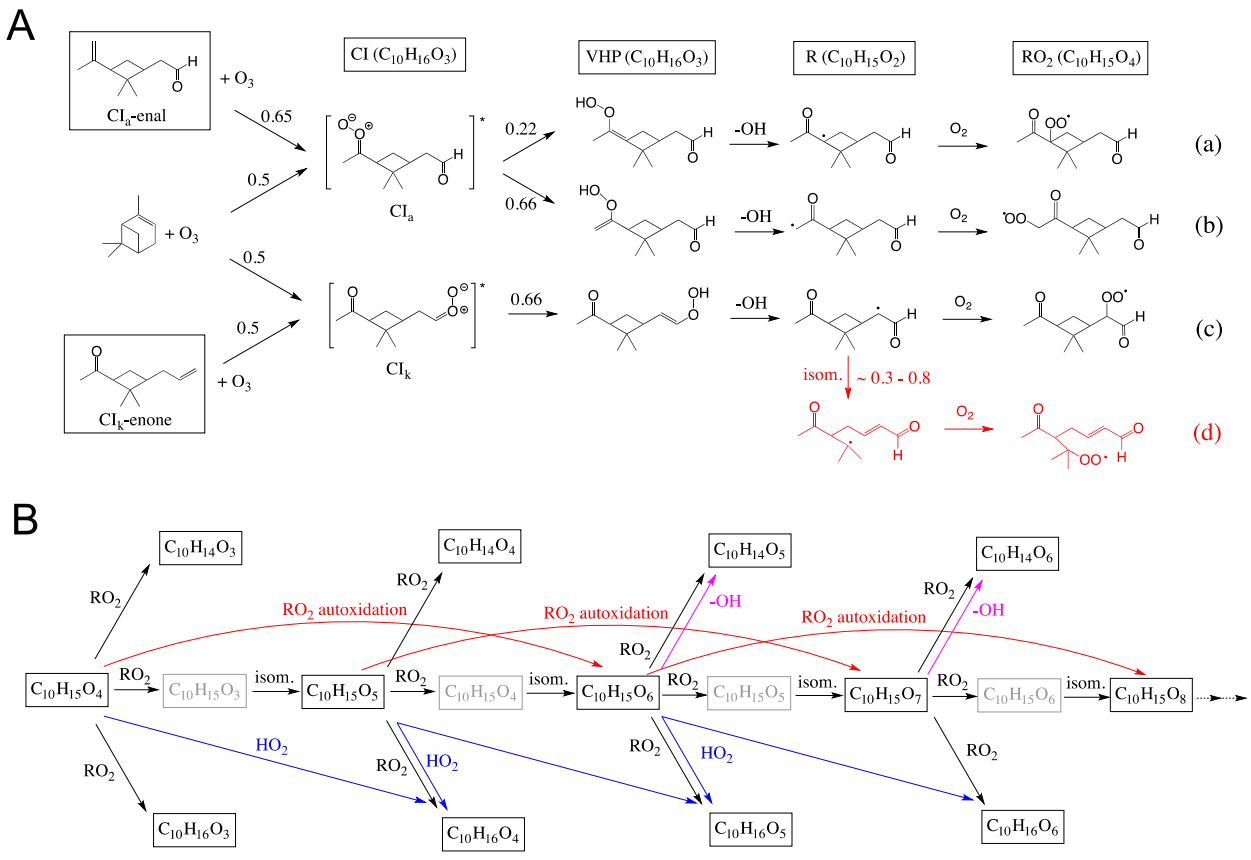

595

596 **Figure 1**. (**A**) Initial ozonolysis reactions of α-pinene, CI_k-enone, and CI_a-enal that lead to
597 formation of four $C_{10}H_{15}O_4$• isomers. The pathway shown in red forms a ring-opened $C_{10}H_{15}O_4$•
598 isomer.[21] The branching ratios shown in the scheme are based on Claflin et al.[38] and Iyer et al.[21]
599 (**B**) The RO_2 bimolecular and unimolecular (i.e., autoxidation) reaction schemes initiated by
600 $C_{10}H_{15}O_4$•. The measured RO_2 and closed-shell products are shown in black text; RO are shown
601 in grey text. The colored arrows represent RO_2 + RO_2 reactions (black), RO_2 + HO_2 reactions
602 (blue), autoxidation reactions (red), and RO_2 termination by loss of OH (pink).[13]

603

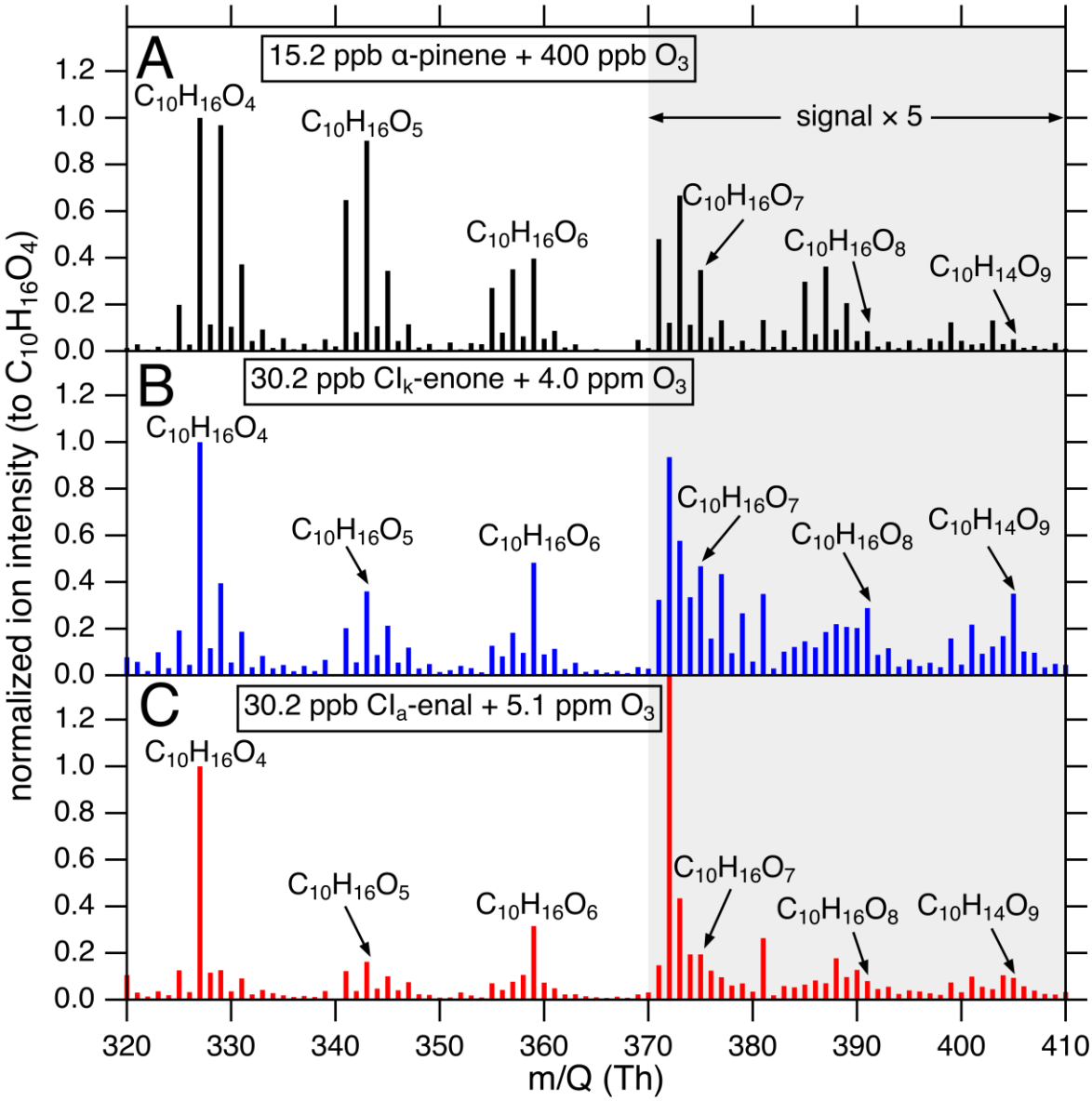

604

605 **Figure 2**. I–CIMS mass spectra (*m/Q* 320 – 410 Th) from the ozonolysis experiments: (**A**) 15.2

606 ppb α-pinene + 400 ppb O_3; (**B**) 30.2 ppb CI_k-enone + 4 ppm O_3; and (**C**) 30.2 ppb CI_a-enal + 5.1

607 ppm O_3. The mass spectra were collected under steady state in the CFSTR.

608

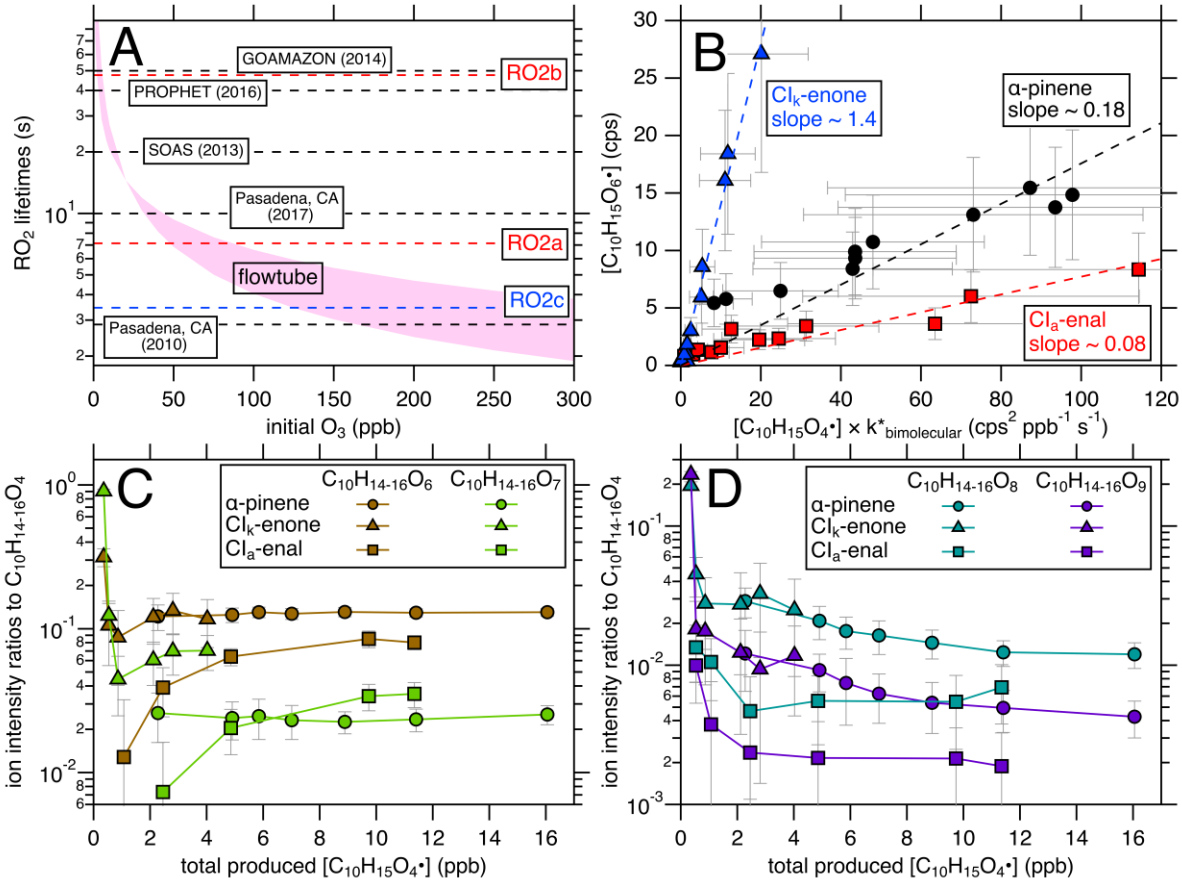

609

610 **Figure 3**. (**A**) RO_2 bimolecular lifetimes (s) simulated under the studied flowtube conditions (pink)
611 and estimated from a few ambient measurements (black dashed lines).[6, 39-42] The shaded region
612 represents the variation using different OH scavengers. In comparison, the reported unimolecular
613 lifetimes of the three $C_{10}H_{15}O_4$• isomers with the cyclobutyl ring are also shown (red and blue
614 dashed lines; RO_2a, RO_2b, and RO_2c correspond to the structures shown in **Figure 1A**).[20] (**B**) The
615 measured $C_{10}H_{15}O_6$• intensities in the flowtube experiments as a function of the $C_{10}H_{15}O_4$•
616 bimolecular reaction rates ($k^*_{bimolecular} = k_{RO2+HO2} \times [HO_2] + k_{RO2+RO2} \times [\Sigma RO_2]$) for the three
617 studied VOCs. $[HO_2]$ and $[\Sigma RO_2]$ are represented by the measured ion intensities; (**C – D**) Ion
618 intensity ratios of summed $C_{10}H_{14\text{-}16}O_x$ (x = 6 – 9) to $C_{10}H_{14\text{-}16}O_4$ as a function of the estimated
619 total $C_{10}H_{15}O_4$• production for the studied flowtube experiments. The error bars represent standard

620 deviation (1σ) of the I–CIMS measurements. In (C), the missing data points for CI_a-enal at low

621 $C_{10}H_{15}O_4$• production were because zero values cannot be display in the log-scale plot.

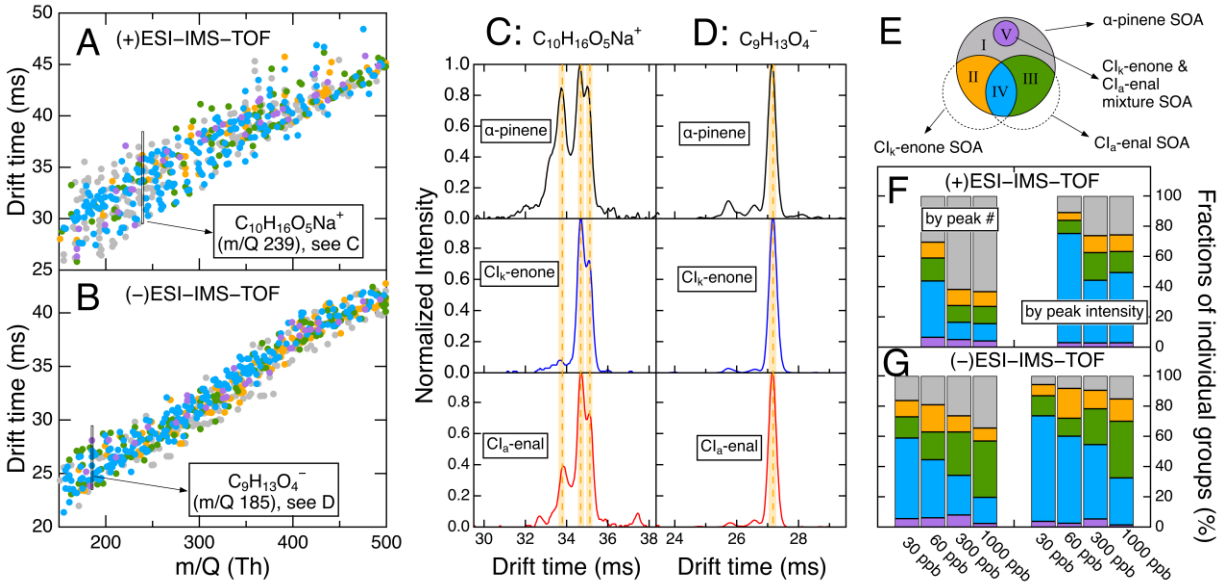

622

623 **Figure 4**. IMS-TOF drift time – *m/Q* diagrams of the SOA constituents from ozonolysis of α-
624 pinene, CI_k-enone, and CI_a-enal with (**A**) (+)ESI and (**B**) (–)ESI. Each symbol represents a single
625 product with unique chemical structure. The *m/Q* range of 150 – 500 Th includes the majority of
626 α-pinene ozonolysis SOA products. The IMS-TOF driftgrams of two representative SOA
627 constituents are shown in (**C**): $C_{10}H_{16}O_5Na^+$ and (**D**): $C_9H_{13}O_4^-$. The vertical dashed lines aligning
628 the large peaks are to guide the eye, with the ± 0.15 ms ranges shown in shaded regions. Shown in
629 the Venn diagram (**E**) is the categorization of the α-pinene ozonolysis SOA constituents into five
630 groups (detail described in the text). (**F**) and (**G**) present the accumulated fractions of each group
631 by peak number and peak intensity, colored based on the categories shown in (**E**). Four
632 experimental conditions are compared, with the initial VOC concentrations shown on the *x*-axis.
633 Only (–)ESI-IMS-TOF measurements were performed for the 30 ppb experiments.

634